Eur. Phys. J. B **30**, 153–160 (2002)
DOI: 10.1140/epjb/e2002-00370-y

THE EUROPEAN PHYSICAL JOURNAL B

Factory-roof-shaped phase front at the paraelectric-ferroelectric transition in KD_2PO_4: an incoherent interface

Z. Kvitek and J. Bornarel[a]

Laboratoire de Spectrométrie Physique [b], Université Joseph Fourier, BP 87, 38402, Saint-Martin d'Hères, France

Received 25 April 2002
Published online 29 November 2002 –

Abstract. The phase front during the 218 K transition in KD_2PO_4 crystals under a thermal gradient $\mathbf{G}_e$ perpendicular to the c ferroelectric axis is observed to have a factory-roof shape. This shape is studied *versus* the magnitude of G_e in samples cut with faces in (100), (010), (001) planes or in $(\bar{1}\bar{1}0)$, (110), (001) ones. A geometric approach as well as the calculation of the elastic-strain energy caused by lattice misfits along the phase front demonstrate the incoherent interface nature of the phase front. Furthemore, the results and their interpretation allow to predict the sign of the lattice deformation u_{xx} (> 0).

PACS. 81.30.Dz Phase diagrams of other materials – 77.80.-e Ferroelectricity and antiferroelectricity – 64.70.-p Specific phase transitions

1 Introduction

KD_2PO_4 (DKDP) crystals undergo a first-order transition between a tetragonal paraelectric and paraelastic phase ($\bar{4}2$ m) which is the high-temperature phase, and an orthorhombic ferroelectric and ferroelastic one (mm2). The polarization P_z that is considered as the order parameter belongs to the B_2 representation as does the shear strain u_{xy} due to the piezoelectricity of DKDP. Besides the shear strain in the plane perpendicular to the ferroelectric c axis, it is possible to observe values of the orthogonal lattice deformation $u_{zz} = 6.5 \times 10^{-4}$ greater in magnitude than u_{xx} and u_{yy} (about 1×10^{-4} in modulus but of unknown polarity) [1,2]. In the low-temperature phase, the permissible walls [3] of the ferroelectric-ferroelastic domains are (100) and (010) tetragonal planes. These domains are also mechanical twins [4] and the mechanical energy plays a great role in the crystal properties correlated to the domains [5].

The character of the DKDP transition was always observed to be first order. It is only during the last ten years that the phase coexistence has been systematically studied in crystals without applied electric field or mechanical stress. Simultaneous dielectric measurements and optical observations of the phase front and the domains allowed for example to understand the different results previously observed on the thermal hysteresis ΔT at the transition [6]: some authors observed ΔT equal to a few tenths of a degree [7,8] and others demonstrated that the phase transition can occur practically without thermal hysteresis [1,9–11]. The explanation is given by occurrence of different phase coexistence phenomena in different experimental conditions of thermal gradient and external electric field or mechanical stress: samples under very small thermal gradient and applied electric field (lower than 300 Vcm^{-1}) exhibit quasiplanar phase fronts during the paraelectric-ferroelectric (PF) cycles as well as during the ferroelectric-paraelectric (FP) ones. On the opposite, when the applied electric field becomes greater than 300 Vcm^{-1} during the FP cycle, the phase front shapes are more complex as coexistence phenomena which induce a higher temperature for the paraelectric phase appear [6].

The phase front shape studies are particularly interesting because of the competition between electrostatic, mechanical and chemical energies. Moreover, owing to the ferroelectric and ferroelastic properties, it is possible to modify their relative importance by application of electric fields, mechanical stresses or thermal gradients respectively. Previous works performed without applied electric field can be summarized as follows:

When the thermal gradient $\mathbf{G}_e$ is small enough, for example 5×10^{-3} Kmm^{-1}, only one or two quasiplanar phase fronts near the (001) plane form during the phase coexistence [11,12]. This result demonstrates the negligible role of the electrostatic energy which is maximum with these electrically charged planes (001). Obviously when the thermal gradient $\mathbf{G}_e$ is greater than 10^{-2} Kmm^{-1} and parallel to the ferroelectric c axis, the phase front is quasiplanar again and near the (001) plane [13]. If the α angle between the thermal gradient $\mathbf{G}_e$ and the c axis increases, more complicated phase front shapes and coexistence phenomena are observed [14]. In all cases each phase front part makes an angle smaller than 25 degrees of arc with the (001) plane. When $\mathbf{G}_e$ is greater than 10^{-2} Kmm^{-1}

[a] e-mail: jean.bornarel@ujf-grenoble.fr
[b] Unité associée au CNRS 8

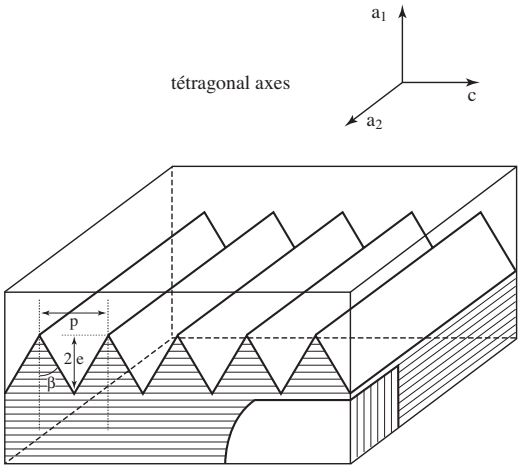

Fig. 1. A schematic illustration of a phase front with a factory-roof shape when $\mathbf{G}_e$ is greater than 10^{-2} Kmm^{-1} and perpendicular to the c axis (along the a_1 axis here).

and perpendicular to the c axis, the phase front forms a factory roof whose section in the a_1 (or a_2) tetragonal planes has a zig-zag shape as shown in Figure 1 [14,15]. In this case, the thermal gradient imposes the ferroelectric state on the lower region of the sample and the paraelectric state on the upper. The factory-roof shaped phase front in the coexistence region appears as the result of competition between mechanical and chemical energies. A theoretical model analyses the competition between the free energy induced by the thermal gradient, the elastic-strain energy caused by lattice misfits along the interface and the interface suface energy [16]. This analysis shows that the formation of a factory-roof shaped phase front is energetically favourable when the ratio of the product of surface and chemical energies to the square of elastic-strain energy is small. When this condition is not satisfied, the interface remains flat. However, this model developed in the approximation of an isotropic medium must be checked against different DKDP results taking into account the anisotropic strains at the transition. Furthermore, an important parameter is the angle β between the planar parts of the phase front and the (001) plane: a constant value of β might suggest that the phase front could be a coherent interface. Therefore in the present paper, the factory-roof shaped phase front (when $\mathbf{G}_e$ is perpendicular to the c axis) is experimentally studied *versus* the $\mathbf{G}_e$ magnitude, during cooling and heating cycles in samples cut with faces in (100), (010), (001) planes or in $(\bar{1}\bar{1}0)$, (110), (001) ones (called tetragonal Te and orthorhombic 0 samples respectively). The results are discussed to clarify the nature of the DKDP phase front: coherent or incoherent interface. In the second case, the elastic energy of the interface is studied with the help of the Khachaturyan theory of inclusions [17].

2 Experimental procedures

The DKDP crystals were grown by slow cooling of a supersaturated solution of KDP and heavy water. The observed transition at 218.1 ± 0.3 K corresponds to a deuteration greater than 99%. The orientations of the sample faces were verified with X-ray Bragg diffraction (accuracy of a minute of arc) for samples prepared as previously described [14]. The experimental results presented here have been obtained with two kinds of samples: the sample Te whose faces are tetragonal planes measures $a_1 = 5.5$ mm, $a_2 = 4.4$ mm, $c = 7.4$ mm; the sample O whose faces are orthorhombic planes measures $a'_1 = 99$ mm ($\mathbf{a}_1 = \mathbf{a}_1 + \mathbf{a}_2$), $a'_2 = 8.9$ mm, $c = 6$ mm.

The DKDP sample was set in a helium-gas exchange chamber of a cryostat allowing optical observations and measurements along three perpendicular axes simultaneously with dielectric measurements. These three axes were perpendicular to the sample faces. The c ferroelectric axis corresponds to a horizontal optical axis. The observations along the a_i (or a'_1) axes allow to rebuild the phase-front shape while the observation along the c axis gives information on the domain texture as illustrated in Figure 1. The thermal gradient $\mathbf{G}_e$ in the helium-gas chamber was vertical and monitored with an accuracy of 5×10^{-3} Kmm^{-1} with the help of two platinum resistors placed just above and below the sample. The temperature reported further on is that of the lower platinum resistor which was measured with a precision of 2×10^{-3} K. Previous papers described the characteristic of this helium-gas exchange chamber [14–18]. Each thermal cycle was performed as follows: the temperature was stabilized for several hours one degree above the temperature of transition. The sample is then cooled regularly during the paraelectric-ferroelectric (PF) cycles to one degree under the transition temperature. The temperature rate equals 0.5×10^{-3} Kmin^{-1} for the sample Te and 1.2×10^{-3} Kmin^{-1} for sample O. Then the temperature is decreased and the sample is kept for 12 hours at a temperature 15 degrees under the transition temperature which simplifies and stabilizes the domain texture. Finally, the temperature is increased during the ferroelastic-paraelastic (FP) cycles at the same rates as during cooling for the same temperature ranges.

The photographs in Figure 2 correspond to observations in a a_2 section during PF cycles under an external thermal gradient $G_e = 0.5$ Kmm^{-1} with the DKDP sample Te set on a window glass. As the thermal conductivity of the glass is similar to that of the crystal, the ferroelectric daggers can appear at each place of the lower a_1 sample face which is also the lowest temperature region (photographs A and B). In photograph C, the zig-zag phase front leaves the a_1 sample face. Then the phase front crosses the sample in the a_1 direction (between C and E) without any shape modification. The simultaneous measurements of the zig-zag position and of the temperature allow to calculate the internal thermal gradient $\mathbf{G}_i$ (equal to 0.1 Kmm^{-1} in this case). In photograph E, the phase front reaches the upper a_1 sample face, which is the warmest one. In the example of Figure 2, this face is surrounded by helium gas and the isotherm curves are perturbed in the sample corners [14]. The results that are given further on concern displacements of the phase front in the middle of the sample where G_i is constant and where the phase-front shape is reproducible.

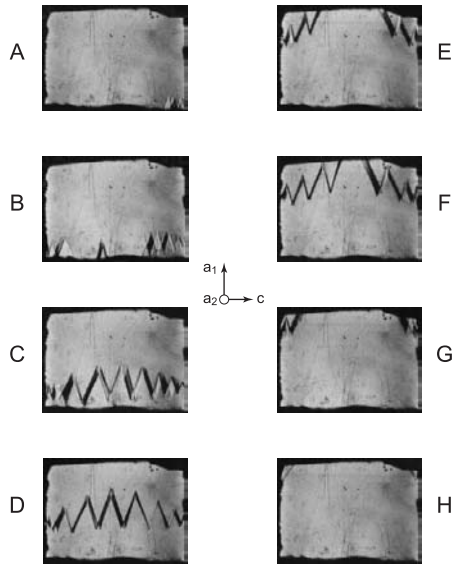

Fig. 2. Phase front shape in a_2 section during a PF transition with $\mathbf{G}_e$ perpendicular to the c axis.

During the phase coexistence it is possible to study the domain texture by observation in a c section or with the help of the diffraction pattern obtained with a laser beam propagating in this c direction [19]. For example, it has been shown that at the beginning of a PF cycle (between A and C) the ferroelectric region remains almost monodomain, which never happens during a FP cycle. Furthemore, semitransparent gold electrodes were evaporated on the c sample faces and two thin copper wires glued with a spot of silver paste allow electrical contacts for dielectric measurements. The dielectric constant ε_c' and the loss constant ε_c'' are then measured with a small a.c. field (1 Vcm^{-1}, 1 kHz) during the experiment. The correlation between the dielectric properties and the coexistence phenomena has been studied elsewhere [11,20]. Here, as shown in Figure 3, these measurements (which correspond to the photographs in Fig. 2) allow to obtain information on the sample quality and to check the reproducibility of the results given in the next section.

3 Results

The results given in this section, during PF and FP cycles, correspond to phase fronts moving very regularly with the temperature variation in the middle of the sample. Their shape remains constant during their motion of a few millimeters while the measured dielectric constant ε_c' keeps its value. Photographs in Figure 4 show phase fronts in sections a_2 and a_1 (left and right photographs respectively) in the sample Te during PF cycles. The parameter is the external thermal gradient magnitude G_e varying between 0.2 Kmm^{-1} and 3 Kmm^{-1}. If G_e is smaller, the phase front crosses all the sample in a a_1 direction and exhibits one or two quasiplanar shapes [11]. If G_e is greater, a zig-zag shape is still obtained but it is difficult to observe a constant internal $\mathbf{G}_i$ value along a few

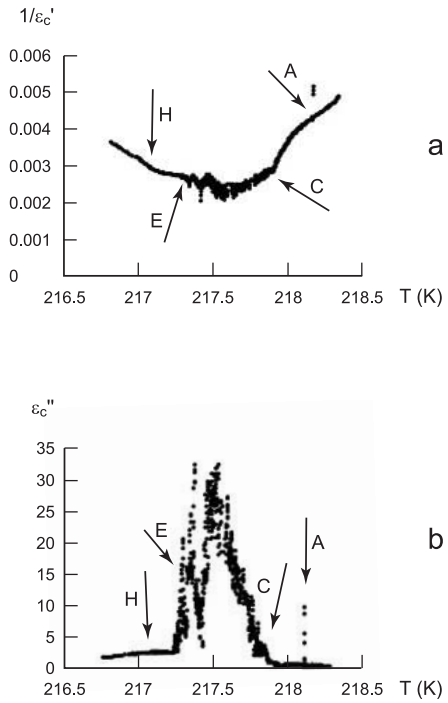

Fig. 3. Temperature variation of ε' and ε'' during the PF transition illustrated in Figure 2. The ferroelectric nuclei appear in A and the last paraelectric nucleus disappears in H. C and E correspond to separation of the zig-zag front from the a_1 sample faces.

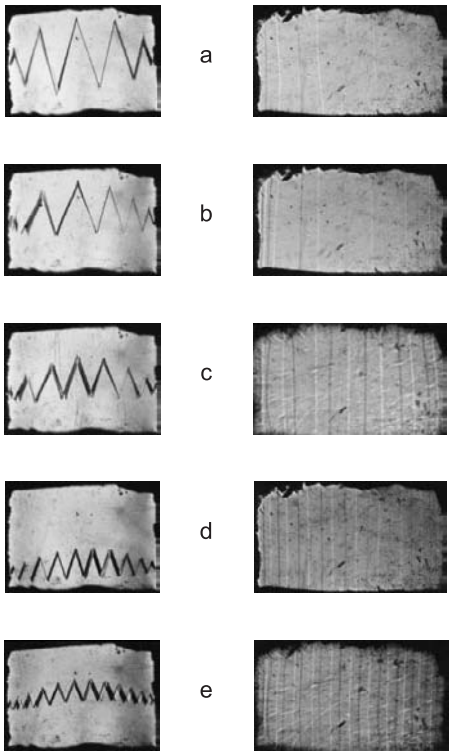

Fig. 4. Photographs of the phase front in the middle of the sample Te in sections a_2 and a_1 (left and right photographs respectively) during PF cycles. The thermal gradient $\mathbf{G}_e$ is perpendicular to c with magnitudes: a = 0.2 Kmm^{-1}, b = 0.5 Kmm^{-1}, c = 1 Kmm^{-1}, d = 2 Kmm^{-1}, e = 3 Kmm^{-1}.

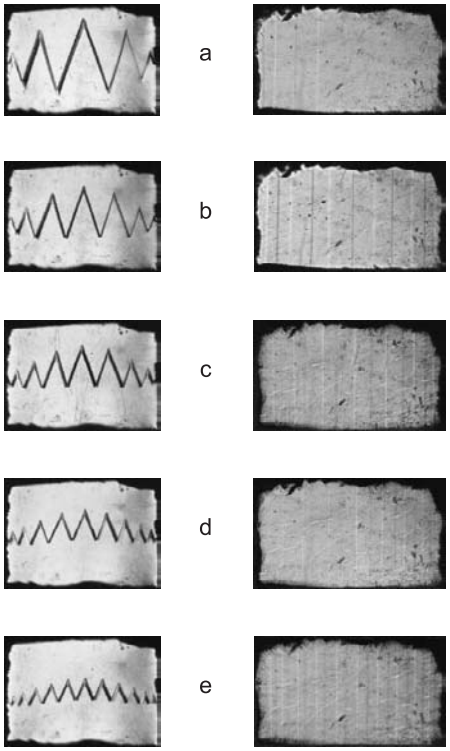

Fig. 5. Photographs of the phase front in the middle of the sample Te in sections a_2 and a_1 (left and right photographs respectively) during FP cycles. The thermal gradient $\mathbf{G}_e$ is perpendicular to c with magnitudes: $a = 0.2$ Kmm^{-1}, $b = 0.5$ Kmm^{-1}, $c = 1.2$ Kmm^{-1}, $d = 2$ Kmm^{-1}, $e = 3$ Kmm^{-1}.

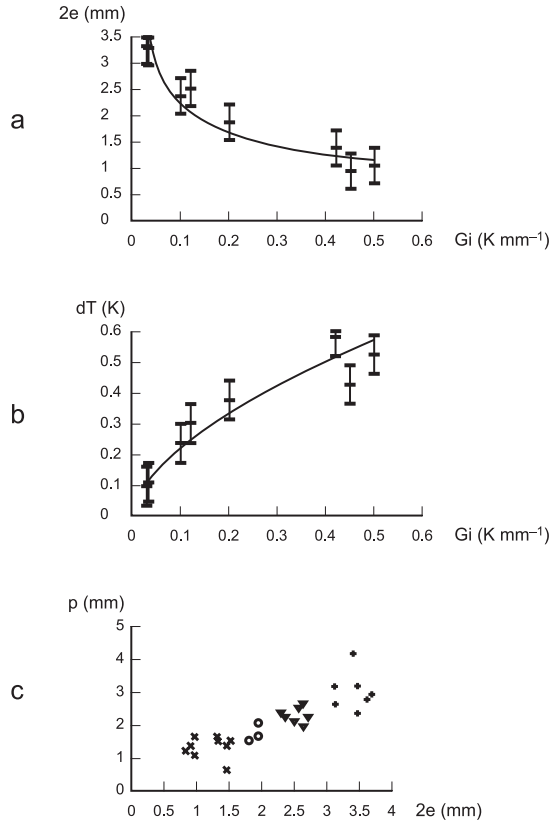

Fig. 6. Sample Te: the effect of the internal thermal gradient G_i during PF cycles and FP cycles on $2e$ (a) and on the coexistence interval δT (b). Variation of p *versus* $2e$ in these different situations (c).

millimeters in a_1 direction. In Figure 5, the same photographs have been taken in similar experimental conditions (0.5×10^{-3} Kmin^{-1} for temperature rate, similar G_e values) during FP cycles. During these PF and FP cycles, the relation between G_i and G_e [14] is found equal to: $G_i = 0.167\ G_e$. The study of the phase front shapes during each thermal cycle *versus* the temperature gradient G_i allows to draw the curves shown in Figure 6. In Figure 6a, the decrease of $2e$, the height of the central triangle of a zig-zag front, as G_i increases is shown. In Figure 6b, the increase of the coexistence interval δT when G_i increases is presented. Finally, in Figure 6c, the variation of p, the basis of the central triangle of a zig-zag front *versus* its height $2e$ is plotted. Each dot on these representations has been obtained in a specific thermal cycle (PF or FP) which explains the dot dispersion. The slope of the dependence between p and $2e$ allows to calculate the angle β between a phase front part and the (001) plane. The result obtained in Figure 6c is $\beta = 25° \pm 5°$.

The previous results have been obtained with the sample Te whose faces are perpendicular to the tetragonal axes. Similar experiments performed with the sample O with faces in orthorhombic planes are illustrated in Figures 7 and 8 (during the corresponding PF and FP cycles, the relation between G_i and G_e is $G_i = 0.213\ G_e$). The β angles observed in case O are always smaller than in case Te as illustrated in Figure 8c where $\beta = 18° \pm 4°$. The

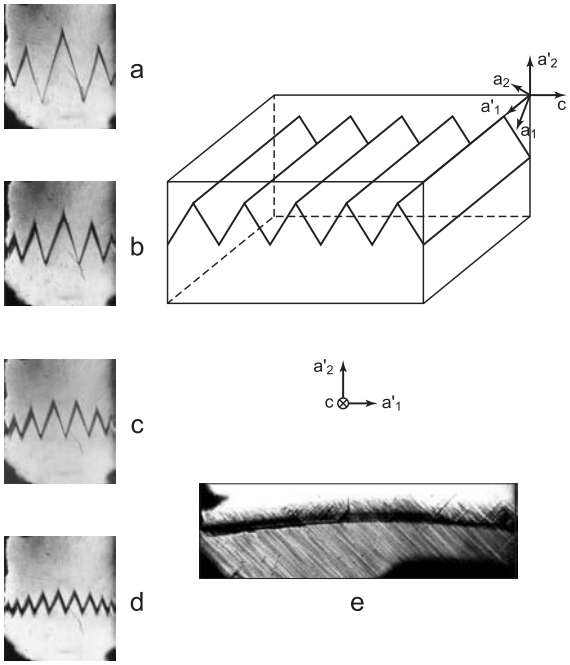

Fig. 7. Photographs of the phase front in the middle of the sample O in a_1' section ($\mathbf{a}_1' = \mathbf{a}_1 + \mathbf{a}_2$) during PF cycles with different G_e values: $a = 0.12$ Kmm^{-1}, $b = 0.33$ Kmm^{-1}, $c = 0.8$ Kmm^{-1}, $d = 2.4$ Kmm^{-1}; (e) photograph of the domains in c section with $G_e = 2.4$ Kmm^{-1}.

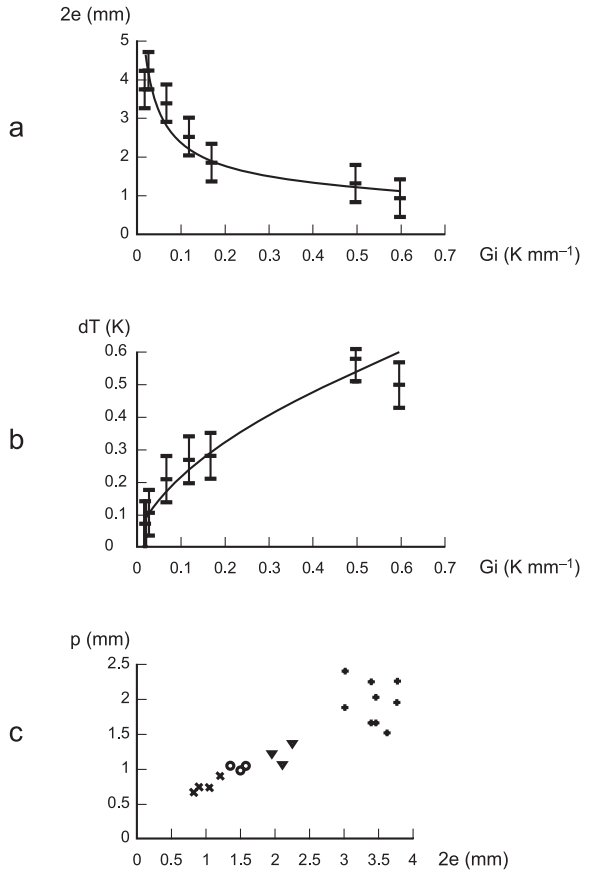

Fig. 8. Sample O: the effect of G_i during PF and FP cycles on $2e$ (a) and on δT (b). Variation of p *versus* $2e$ in these different situations (c).

lines of the zig-zag ridges are thicker in Figure 7 than in Figures 4 or 5 especially for large G_i values. The explanation is given in Figure 7e where the observation along the c axis shows curved ridges of the zig-zags in the O case, while in the Te case straight ridges are observed. This phenomenon can be the result of thermal or strain distributions. To summarize, the zig-zag shapes of the phase fronts during PF and FP cycles, with O and Te samples where $\mathbf{G}_e$ is perpendicular to the c axis are observed to be similar in the middle of the samples. The most important feature is that the angle β between a phase front part and the (001) plane is smaller in sample O (with faces in orthorhombic planes) than in sample Te (with faces in tetragonal planes).

4 Discussion

The zig-zag shape of the phase front has been explained with the help of a model taking into account the energy induced by a thermal gradient perpendicular to the c axis (chemical energy), the elastic-strain energy caused by lattice misfits due to the phase front existence and the interface surface energy [16]. It has been shown that the zig-zag-shaped interface is energetically favourable when the product of terms related to surface and chemical energies is small enough in relation to the square of the elastic-strain energy term. The important role of the elastic-strain energy density corresponding to a quasiplanar phase front part is demonstrated. The aim of the present paper is to clarify this energy term. Firstly, coherent interface solutions are considered; secondly, the bulk energy due to a quasiplanar inclusion is studied.

The orientation of a coherent interface corresponds to planes where deformations in the two phases are equal. Then, no long range stress is created by such an interface. To define the equation of the interface plane, one writes that a vector connecting two points in phase I is conserved in phase II. This procedure has been much used to determine allowed domain walls in ferroelectric [3] and ferroelastic [21] crystals and also phase fronts in different transitions [22–24]. For example, in DKDP crystals, the allowed ferroelectric walls are found to be the (100) and (010) planes. It is a little more difficult to determine the possible coherent phase fronts between the tetragonal phase and the orthorhombic one: it is necessary to take into account the domain species and their proportion to calculate the appropriate value of the macrostrain S in phase II related to phase I.

Firstly, the tensors which express the deformation and the rotation are written, for example for domains whose walls are in (100) planes and for both polarities + and −.

$$D_x^+ = \begin{vmatrix} u_{xx} & 0 & 0 \\ u_{xy} & u_{xx} & 0 \\ 0 & 0 & u_{zz} \end{vmatrix}, \qquad D_x^- = \begin{vmatrix} u_{xx} & 0 & 0 \\ -u_{xy} & u_{xx} & 0 \\ 0 & 0 & u_{zz} \end{vmatrix}.$$

If the ratio between the volume of the + domains and the total volume of the ferroelectric phase is m, the macrodistortion of this phase is described by

$$D_x = m\, D_x^+ + (1-m)\, D_x^- .$$

But only the symmetric part of this tensor gives a macrodeformation S_x:

$$S_x = \begin{vmatrix} u_{xx} & u_{xy}\left(m-\frac{1}{2}\right) & 0 \\ u_{xy}\left(m-\frac{1}{2}\right) & u_{xx} & 0 \\ 0 & 0 & u_{zz} \end{vmatrix}.$$

The macrodeformation S_y relating to domains whose walls are in (010) planes equals $S_x (S_y = S_x = S)$, and the orientation of the coherent interface is defined by the following equation

$$\mathrm{d}\mathbf{r} \cdot S \cdot \mathrm{d}\mathbf{r} = 0,$$

where $\mathbf{r}$ corresponds to the position of a point of the phase front. A solution is obtained when

$$u_{zz} \cdot u_{xx} < 0 \text{ and } \det|S| = 0,$$

which leads to

$$u_{xx}^2 - u_{xy}^2 \left(m-\frac{1}{2}\right)^2 = 0.$$

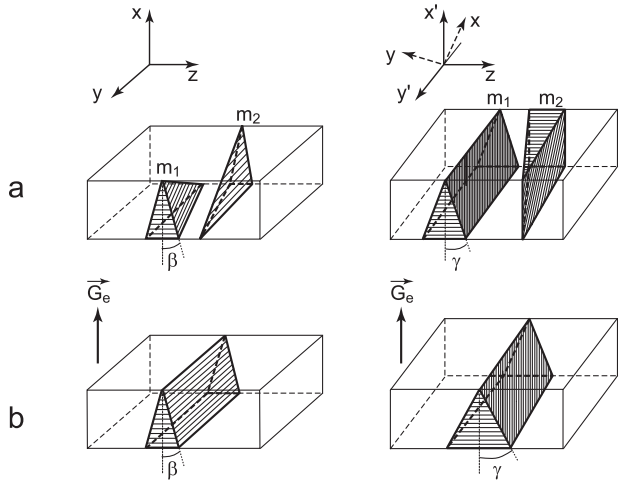

Fig. 9. A schematic illustration of theoretical phase front orientation in samples Te (left) and O (right). (a) coherent interfaces without applied $\mathbf{G}_e$, (b) possible phase-front shape in samples under $\mathbf{G}_e$.

It is well known that $u_{zz} > 0$. Thus, for a coherent interface u_{xx} must be negative. The solutions are

$$m_1 = \frac{1}{2} - \frac{u_{xx}}{u_{xy}},$$

$$\text{then } S_x^{(1)} = S_y^{(1)} = S^{(1)} = \begin{vmatrix} u_{xx} & -u_{xx} & 0 \\ -u_{xx} & u_{xx} & 0 \\ 0 & 0 & u_{zz} \end{vmatrix},$$

$$\text{and } m_2 = \frac{1}{2} + \frac{u_{xx}}{u_{xy}},$$

$$\text{then } S_x^{(2)} = S_y^{(2)} = S^{(2)} = \begin{vmatrix} u_{xx} & u_{xx} & 0 \\ u_{xx} & u_{xx} & 0 \\ 0 & 0 & u_{zz} \end{vmatrix}.$$

The macrostrain S can also be written in the orthorhombic axes which are eigenvectors of S

$$S^{(1)} = \begin{vmatrix} 2u_{xx} & 0 & 0 \\ 0 & 0 & 0 \\ 0 & 0 & u_{zz} \end{vmatrix} \text{ and } S^{(2)} = \begin{vmatrix} 0 & 0 & 0 \\ 0 & 2u_{xx} & 0 \\ 0 & 0 & u_{zz} \end{vmatrix}.$$

The possible phase front orientations are shown in Figure 9a for samples Te (left) and O (right). In sample Te with domain walls perpendicular to x, the dagger m_1 exhibits a polarization $+(m_1 = \frac{1}{2} - \frac{u_{xx}}{u_{xy}})$ and the dagger m_2 a polarization $-(m_2 = \frac{1}{2} + \frac{u_{xx}}{u_{xy}})$. Those polarizations would be exchanged if the daggers contained domain walls perpendicular to y. It is easy to calculate the angle β in Figure 9a (left): $\beta = \text{arctg}[\frac{|u_{xx}|}{u_{zz}}]^{1/2} = 21.4$ degrees of arc while the angle γ in Figure 9a (right): $\gamma = \text{arctg}[\frac{2|u_{xx}|}{u_{zz}}]^{1/2} = 29$ degrees of arc (in the previous case the m_1 and m_2 values are 0.51 and 0.49, respectively). Then the angle between the coherent interface and the (001) plane is greater in sample O than in sample Te, contrary to the experimental observations. However, the experimental results are obtained with an applied thermal gradient $\mathbf{G}_e$. What can its effect be? In sample O, as shown in Figure 9b (right), the dagger m_2 becomes improbable. In sample Te, the dagger shown in Figure 9b (left) appears as a mean between dagger m_1 and m_2 of Figure 9a (left) and the phase front is an incoherent interface. Then, one can conclude that the hypothesis of coherent interfaces for the phase front must be given up.

As the geometric approach is not appropriate, it is necessary to minimize the free energy. The elastic-strain energy due existence of the phase front plays an important role. This energy depends directly on the energy density B of an infinitesimally thin plate-like inclusion of phase II in an infinite medium of phase I. As shown in reference [16], the energy of an inclusion can be written:

$$E_{\text{bulk}} = \frac{1}{2} B(\mathbf{n}) V, \tag{1}$$

where V is the inclusion volume, $\mathbf{n}$ the normal to the inclusion plane, and B the energy density per unit length in the direction z taken here as the c axis direction. With the help of previous works [16] using the Khatchaturyan theory [17,22], it leads to

$$B(\mathbf{n}) = \lambda_{ijkl}\, u_{ij}\, u_{kl} - n_i\, \sigma_{ij}\, \Omega_{jl}\, \sigma_{em}\, n_m,$$
$$\text{with } \sigma_{ij} = \lambda_{ijkl}\, u_{kl} \text{ and } \Omega_{jl}^{-1} = \lambda_{qjpl}^{npnq}$$

where λ_{ijkl} are the elastic constants and u_{ij} and σ_{ij} the mechanical strain and stress components, respectively.

Previous works of different authors give λ_{ijkl} and u_{ij} values near the transition (usual notations for indices correspond to $x = 1$, $y = 2$, $z = 3$):

$u_{11} = u_{22} = 1 \times 10^{-4}$ (Ref. [25]),
$u_{33} = 6.5 \times 10^{-4}$ (Ref. [26]),
$\lambda_{1111} = \lambda_{2222} = 7.2 \times 10^{10}$ N m^{-2},
$\lambda_{1122} = -1 \times 10^{10}$ N m^{-2},
$\lambda_{1313} = \lambda_{2323} = 1.2 \times 10^{10}$ N m^{-2},
$\lambda_{3333} = 5.4 \times 10^{10}$ N m^{-2},
$\lambda_{1133} = \lambda_{2233} = 1.2 \times 10^{10}$ N m^{-2} (Ref. [27]),
$\lambda_{1212}^{P} = 0.6 \times 10^{10}$ N m^{-2} (Ref. [28]),
$u_{12} = 7.2 \times 10^{-3}$ (Ref. [26])
or 9.6×10^{3} N m^{-3} (Ref. [29]).

It is then possible to calculate B as a function of the angle β between $\mathbf{n}$ and the ferroelectric axis c.

The variation of B *versus* β is given in Figure 10 with the sign of u_{xx} and the $\mathbf{G}_e$ orientation as parameters. Three orientations of $\mathbf{G}_e$ are considered: the orthorhombic axes $\mathbf{a}_1' = \mathbf{a}_1 + \mathbf{a}_2$ and $\mathbf{a}_2' = \mathbf{a}_1 - \mathbf{a}_2$, and the tetragonal axis $\mathbf{a}_1$ (or $\mathbf{a}_2$). The variation of m *versus* β is also given on the same graph which allows to know what value of m is used in the calculation of B. For the negative sign of u_{xx}, the geometric results of Figure 9a (right) are confirmed with

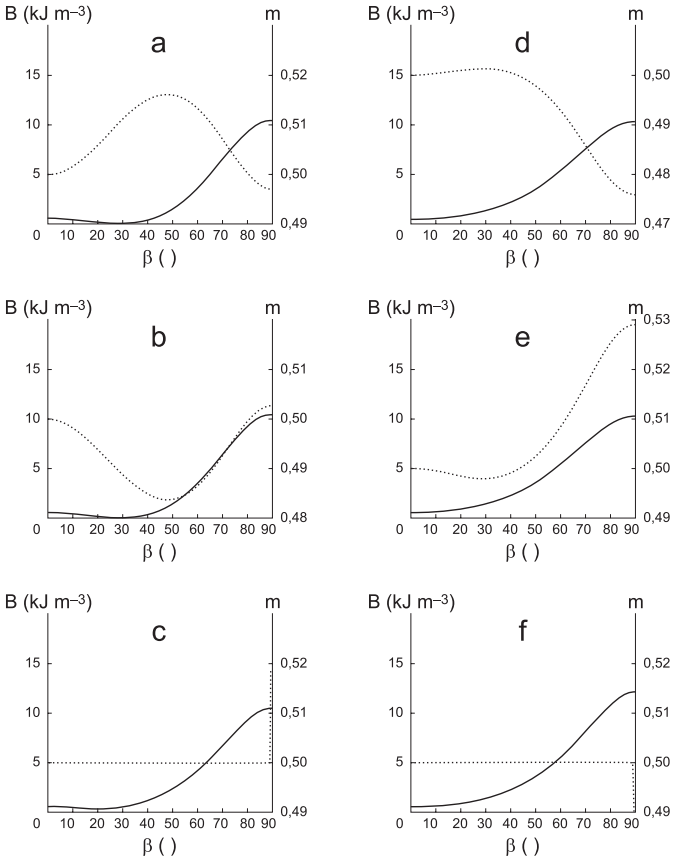

Fig. 10. Variation of B (continuous lines) energy density per unit length along c *versus* β angle between a phase front part and the (001) plane. The parameters are the sign of u_{xx} and the $\mathbf{G}_e$ orientation: $u_{xx} = -1 \times 10^{-4}$ in a, b, c with $\mathbf{G}_e$ along $\mathbf{a}_1 + \mathbf{a}_2$, $\mathbf{a}_1 - \mathbf{a}_2$, $\mathbf{a}_1$ respectively. On the same curves is also drawn the variation of m, ratio of the + domains volume and the total volume of the ferroelectric phase (dotted lines).

$\mathbf{G}_e$ parallel to $\mathbf{a}'_1$ and $\mathbf{a}'_2$: B exhibits a zero minimum value at β equals 29 degrees of arc in Figures 10a and b (with m equalling 0.49 and 0.51 respectively). In these particular cases the interface is coherent. If $\mathbf{G}_e$ is parallel to $\mathbf{a}_1$ like in Figure 10c, B exhibits a nonzero minimum value at β equals 20 degrees of arc. The interface is incoherent and the macrostrain (or macropolarization) remains zero because $m = 0.5$ for all the β values.

Curves $B(\beta)$ and $m(\beta)$ are also drawn for positive sign of u_{xx} in Figures 10d, e, f. The B minimum value is not zero and it is obtained when β equals zero (with m equalling 0.499, 0.501 and 0.5 for $\mathbf{G}_e$ parallel to $\mathbf{a}'_1$, $\mathbf{a}'_2$, $\mathbf{a}_1$ respectively). Then the interface is always incoherent. These calculated results are in good agreement with the experimental observations of phase fronts perpendicular to c axis ($\beta = 0$ when $G_e = 0$) [11].

The Figure 10 results allow to conclude the following: the sign of u_{xx} cannot be negative because the calculated β angles (29 and 20 degrees of arc) are not compatible with the experimentally observed values (18 and 25 degrees of arc respectively). On the contrary a good agreement is obtained with a positive sign for u_{xx} .

Results given in Figures 6 and 8 allow to check the model of the zig-zag-shaped interface previously published by one of the authors (Z.K.) [16]. In the approximation of an isotropic and infinite medium, an interface as shown in Figure 1 can be explained as resulting from the competition between the free energy induced by the gradient $\mathbf{G}_e$, the elastic-strain energy caused by lattice misfits along the interface, and another energy like an interface surface energy. The total energy density ρ per unit length along the c axis can then be written (relation (6) of Ref. [16]):

$$\rho = \rho_{cH} + \rho_{es} + \rho_s, \tag{2}$$

with ρ_{cH} the chemical energy density equal to $\frac{1}{6} G_i |\Delta S| e^2$, where $|\Delta S|$ is the jump in entropy at the transition, with ρ_{es} the elastic-strain energy density equal to $\frac{eA(\beta)}{6}$, where $A(\beta) = B(\beta = 90°) - B(\beta)$, and with ρ_s the surface energy density equal to $(\frac{1}{\sin\beta} - 1)\gamma$ if a constant surface energy γ of the interface is assumed. The minimization of ρ for a given β value allows to obtain

$$2e = \frac{A(\beta)}{|\Delta S|} \frac{1}{G_i} \text{ and } \delta T = 2eG_i = \frac{A(\beta)}{|\Delta S|} \cdot \tag{3}$$

These variations of $2e$ and δT *versus* G_i are not in good agreement with the experimental results of Figures 6 and 8 where $2e \approx G_i^{-1/n}$ and $\delta T \approx G_i^{(1-1/n)}$ (n equals approximately 2). Thus the approximations of an isotropic and infinite medium and of an interface as shown in Figure 1 do not account of the e and δT variations with G_i. For example, there is no evidence of the ρ_s term with a constant γ value. The most inadequate hypothesis is the planar envelope of the factory-roof edges which induces the term $B(\beta = 90°)$ in the parameter $A(\beta)$. This envelope is nearly planar when the G_i magnitude equals a few Kmm^{-1} as shown in Figures 4, 5 and 7. On the opposite for smaller G_i values the envelope is curved and the influence of the sample boundaries is evident. The study of the envelope curvature and the β variation in function of the G_e magnitude is currently in progress. The influence of a small dc electric field which changes the m values is also observed. Further models will take into account the relaxation of the stresses at the sample boundaries.

5 Conclusion

Observations of the phase front and the domains during PF and FP transitions have been performed in KD_2PO_4 crystals under a thermal gradient perpendicular to the c ferroelectric axis. The samples have been cut with their faces in tetragonal or orthorhombic planes (Te or O samples). The phase front appears as a factory-roof whose β angles between planar parts of the phase front and the (001) plane are greater in Te samples than in the O samples (25 and 18 degrees of arc, respectively). This demonstrates that DKDP phase fronts are not coherent interfaces. The elastic-strain energy caused by lattice misfits of this incoherent interface has been shown as minimum

in the (001) plane, in agreement with results obtained for samples under negligible thermal gradient. The sign of the lattice deformation u_{xx} is determined as positive. The factory-roof shapes are well explained as result of the competition between the chemical energy and the mechanical one in which the elastic-strain energy plays the greater role.

References

1. C.M.E. Zeyen, H. Meister, W. Kley, Solid State Comun. **18**, 621 (1976)
2. C.M.E. Zeyen, H. Meister, Ferroelectrics **14**, 731 (1976)
3. J. Fousek, V. Janovec, J. Appl. Phys. **40**, 135 (1969)
4. J. Bornarel, J. Lajzerowicz, J. Appl. Phys. **39**, 4339 (1968)
5. J. Bornarel, J. Appl. Phys. **43**, 3845 (1972)
6. Z. Kvitek, J. Bornarel, J. Phys. Cond. Matt. **12**, 7819 (2000)
7. E.V. Sidnenko, W. Gladkii, Sov. Phys-Crystalogr. **17**, 861 (1973)
8. M. Chabin, F. Gilletta, Ferroelectrics **15**, 149 (1977)
9. W. Reese, L.F. May, Phys. Rev. **167**, 504 (1968)
10. W. Reese, Phys. Rev. **181**, 905 (1969)
11. J. Bornarel, R. Cach, Phys. Rev. **60**, 3806 (1999)
12. Z. Kvitek, J. Bornarel, Ferroelectrics **190**, 31 (1997)
13. J. Bornarel, R. Cach, J. Phys. Cond. Matt. **5**, 2977 (1993)
14. J. Bornarel, R. Cach, Z. Kvitek, J. Phys. Cond. Matt. **8**, 7365 (1996)
15. J. Bornarel, R. Cach, Ferroelectrics **124**, 345 (1991)
16. Z. Kvitek, J. Phys. Cond. Matt. **9**, 127 (1997)
17. A.G. Khachaturyan, *Theory of Structural Transformations in Solids* (Wiley-Interscience, New York, 1983)
18. J. Bornarel, R. Cach, J. Phys. Cond. Matt. **6**, 1663 (1994)
19. R.M. Hill, S.K. Ichiki, Phys. Rev. A **135**, 1640 (1964)
20. J. Bornarel, R. Cach, Z. Kvitek, J. Phys. Cond. Matt. **8**, 11337 (1996)
21. J. Sapriel, Phys. Rev. B **12**, 11, 5128 (1975)
22. A.G. Khachaturyan, Sov. Phys. Solid State **8**, 2163 (1967)
23. A.L. Roytburd, Sov. Phys. Usp. **17**, 3, 326 (1974)
24. J. Dec, Phase Transitions **45**, 35 (1993)
25. Aleshko-Ozhevskij, Sov. Phys. Solid State **34**, 934 (1992)
26. C.M.E. Zeyen, H. Meister, Ferroelectrics **14**, 731 (1976)
27. *Landolt-Börnstein New Series Ferroelectrics III* (Springer, Berlin)
28. E. Litov, E.A. Vehling, Phys. Rev. B **1**, 3713 (1970)
29. R.J. Nelmes, Z. Tun, W.F. Kuhns, Ferroelectrics **71**, 125 (1987)